Solution Structures of Human Transforming Growth Factor α Derived from ^1H NMR Data†

Tammy Page Kline,* Frank K. Brown,‡ Stephen C. Brown,‡ Peter W. Jeffs,‡ Kenneth D. Kopple, and Luciano Mueller§

Smith Kline & French Laboratories, Mail Code L-940, P.O. Box 1539, King of Prussia, Pennsylvania 19406-0939

Received January 31, 1990; Revised Manuscript Received April 25, 1990

ABSTRACT: The 600-MHz ^1H NMR spectrum of the des-Val-Val mutant of human transforming growth factor α (TGF-α) was reassigned at pH = 6.3. The conformation space of des-Val-Val TGF-α was explored by distance geometry embedding followed by restrained molecular dynamics refinement using NOE distance constraints and some torsion angle constraints derived from *J*-couplings. Over 80 long-range NOE constraints were found by completely assigning all resolved cross-peaks in the NOESY spectra. Low NOE constraint violations were observed in structures obtained with the following three different refinement procedures: interactive annealing in DSPACE, AMBER 3.0 restrained molecular dynamics, and dynamic simulated annealing in XPLOR. The segment from Phe15 to Asp47 was found to be conformationally well-defined. Back-calculations of NOESY spectra were used to evaluate the quality of the structures. Our calculated structures resemble the ribbon diagram presentations that were recently reported by other groups. Several side-chain conformations appear to be well-defined as does the relative orientation of the C loop to the N-terminal half of the protein.

Human transforming growth factor α (TGF-α) is a 50-residue polypeptide secreted by many transformed cell lines (De Larco et al., 1978; Ozanne et al., 1980; Kaplan et al., 1981, 1982), cancer cells (Derynck et al., 1986, 1987), and embryonic cells (Ozanne et al., 1980; Todaro et al., 1980; Twardzik et al., 1982). As a member of the epidermal growth factor (EGF) like family of growth factors, TGF-α exerts most of its observed biological activities via binding to the EGF receptor. However, it has been shown that EGF and TGF-α have different activities in some tissues and do not compete with the same receptors for these activities (Abdullah et al., 1989). TGF-α has been implicated as a potential autocrine or paracrine factor involved in maintaining the growth of some human cancers, particularly colon (Murthy et al., 1989) and breast tumors. Reduction of any of the three disulfide bonds leads to a sharp drop in binding and activity, while reduction of all three disulfide bonds completely inactivates the protein, suggesting that a stable tertiary structure is absolutely required. None of the some dozen members of this family of growth factors has yielded well-diffracting crystals for structural analysis. Attempts to separate binding from activity through construction of analogues by site-specific mutagenesis (Purchio et al., 1987; Lazar et al., 1988, 1989; Defeo-Jones et al., 1988) or chemical synthesis (Tam, 1987, 1988) have been as yet unsuccessful but have shown which residues are most important for activity. However, most of these studies cannot differentiate between changes in activity induced by an altered structure of the protein from changes induced by an altered amino acid contacting the receptor. To extrapolate the methods and ideas of standard structure–activity relationships (SAR) to protein–receptor interactions, one must know more about the "S" than is usually obtained. Consequently, we initiated a structural study of TGF-α to complement ongoing mutational analysis studies.

We have reported previously ^1H NMR assignments of TGF-α at pH = 3.4 and identification of secondary structural elements (Brown, S. C., et al., 1989). Our results were in close agreement with the findings of Montelione et al. (1989), who studied the protein under similar conditions. Although our NMR analysis was originally performed at pH = 3.4, subsequent work under more physiological conditions (pH 7.4, 150 mM NaCl) demonstrated markedly enhanced structural stability for the N-terminal residues (1–7) and the "A" loop (residues 9–15) than observed at low pH (S. C. Brown, unpublished results). However, at pH values > 6.8, most amide resonances in the protein were exchanging with the H_2O resonance at rates comparable to the magnetic relaxation rates. To obtain the most complete NOE data set possible under solution conditions that most closely approximated the physiological state, it was found that pH = 6.3 was optimal.

For these reasons, the ^1H NMR spectrum of TGF-α was reassigned at pH = 6.3 and 20 °C in 50 mM sodium phosphate buffer. Assignments were made for all resolved cross-peaks in NOESY spectra that were collected at τ_m = 0.15 and 0.3 s, both in H_2O and in D_2O solutions. Self-consistency and completeness of the combined data were assessed periodically by the template analysis algorithm (Hempel & Brown, 1990). The NOE matrix and torsional angles (from measured $^3J_{H\alpha,H\beta}$) derived from these spectra were converted into structures by using the metric matrix approach. These structures were subsequently refined by several algorithms and protocols. Many side-chain conformations were identified in the final structures. Furthermore, the quality of the structures was periodically checked by making comparisons between experimental and back-calculated NOESY spectra.

Independently, Campbell and co-workers (Tappin et al., 1989) found that TGF-α adopts a slightly different and more stable conformation at neutral and high pH values. Three-dimensional folding of the TGF-α polypeptide chains has been proposed by Kohda et al. (1989), Katz et al. (1989), and

† This work was funded in part by National Institutes of Health Grant GM-39526.

‡ Present address: Glaxo Research, Inc., V-305, 4117 Emperor Blvd., Morrisville, NC 27560.

§ Present address: Squibb Institute for Medical Research, Room D4159, P.O. Box 4000, Princeton, NJ 08543.

0006-2960/90/0429-7805$02.50/0

Campbell et al. (1989). Both Kohda and Campbell presented ribbon diagrams of the peptide backbone of a conformation that fit their NMR data. No details have yet been published of any of these proposed structures or the methods used to generate them and to evaluate their precision and accuracy. In this paper, we report a thorough search of peptide conformations that are compatible with our NMR data (NOE distance constraints and *J*-couplings). We have included the complete input data set in the supplementary material and describe the methods employed in deriving the atomic coordinates of the resulting structures of TGF-α, which are to be made public.

Materials and Methods

NMR Spectroscopy. All structural information was derived from spectra of the des-Val-Val mutant of TGF-α, which were collected on a Bruker AM600 spectrometer at 20 °C. TGF-α was dissolved to a concentration of 3.5 mM in 50 mM phosphate buffer (pH = 6.3), 0.1 mM EDTA, and 0.1 mM NaN_3. Following the completion of a series of spectra in H_2O, the sample was lyophilized on a Speed Vac (Savant) and redissolved in 99.99% D_2O (from MSD Isotopes, St. Louis, MO). This procedure ensured a very good match of cross-peaks in all two-dimensional spectra.

Resonance assignment was performed by using the standard sequential assignment procedure (Wuthrich, 1986): elucidation of type-specific assignments was accomplished by establishing through-bond connectivities among protons with the help of DQF-COSY (Rance et al., 1983), phase-sensitive double-quantum (Wagner et al., 1983; Dalvit et al., 1986), and MLEV-17 (Bax & Davis, 1985) spectra (both in H_2O and in D_2O), followed by sequential linkage of the established *J*-connectivity maps by searching for sequential NOE cross-peaks in NOESY spectra (Wuthrich, 1986, and references therein) collected in H_2O with long mixing times (τ_m = 0.3 s). This analysis resulted in the completion of almost all resonance assignments both in the backbone and in the side chains (a summary of sequential NOE is shown in supplemental figure 1) with the exception of amino resonances whose protons presumably were in rapid exchange with H_2O.

Nonsequential NOE Cross-Peak Assignments. A number of nonsequential NOE cross-peaks were unambiguously assigned in well-resolved regions of the spectrum. Distance constraints were generated from these NOEs by using the following protocol: For distance constraints involving amide and aromatic protons, the lower bounds were uniformly set to 1.8 Å (Wuthrich, 1986) and the upper bounds were set to 2.7 Å for strong, 3.5 Å for intermediate, and 4.5 Å for weak cross-peaks. For most other proton pairs, bounds were estimated from volume integrals, which were obtained by manual peak picking in FTNMR (Hare Research, Inc.). A range of bound was chosen equaling +20%, −15% of the estimated distances, which were obtained by using integrals of internal markers, e.g., $d_{NH_{i+1},d_{C_\alpha H_i}}$ = 2.2 Å in β-sheets, except for weak or overlapping cross-peaks where bounds were estimated qualitatively.

Preliminary structures were built from these distance constraints by using the metric matrix program DSPACE (Hare Research, Inc.). Additional NOE cross-peaks were identified from these preliminary structures with the help of the NOE identification program IDNOE (P. L. Weber, T. P. Kline, and L. Mueller, to be submitted) and by using the redundancy of NOE connectivities caused by spin diffusion in NOESY spectra (Bothner-By et al., 1982) collected with long mixing periods. IDNOE systematically searches for possible assignments for each picked cross-peak in a NOESY spectrum. This is accomplished by computing the distances in the preliminary trial structure for all possible proton pairs that resonate within an interval δ at the frequencies (f_1, f_2) of a selected cross-peak. Prospective parent protons of a cross-peak are most likely separated by less than 5 Å if the overall folding of the peptide chain is properly mapped in the trial structure. Hence, most proton pairs can generally be ruled out as possible NOE assignments due to their large separation in the trial structures. In most cases, unique assignments were found for NOESY cross-peaks. Ambiguities resulting from multiple matches, i.e., more than one proton pair being separated by >5 Å, could be resolved by searching for cross-peaks caused by spin diffusion in NOESY spectra at long mixing times. In these cases, spin diffusion effects a relay of magnetization to more remote neighbors giving rise to a set of additional NOESY cross-peaks, e.g., to the second methyl of a valine or a geminal methylene proton, which then provides redundant connectivity information. This method was used to distinguish between NOEs to Phe ϵ and ξ protons (same approximate chemical shift). Spin diffusion to the δ proton identified all except one of the seven NOEs as due to Phe ϵ. The unresolved NOE (due to spectral overlap) was assigned to the ϵ proton, but the distance constraints were relaxed. IDNOE also lists all unassigned protons that are within a given sphere (4 Å) of an identified proton pair, alerting the user of missing entries in the chemical shift assignment file. A summary of the assignments for TGF-α is given in Table I.

NOEs identified in this process were used to generate more refined structures which then served as new input to IDNOE to confirm present assignments as well as making new ones. We were able to make positive assignments for all resolved NOE cross-peaks both in H_2O and in D_2O spectra. A total of over 380 NOEs were identified as listed in supplemental table S1. Of particular importance to the structure elucidation are the NOEs involving spatially linked protons that are separated by more than one residue along the peptide sequence. A total of 81 such nonsequential NOEs were observed in TGF-α in spectra collected at a mixing time of 0.15 s. Most of these NOEs involve side-chain contacts and only 11 long-range contacts originate from amide protons.

The coupling constants $^3J_{H\alpha,H\beta}$ (Table II) were determined for a number of residues in PECOSY spectra which were collected in D_2O by using the PECOSY sequence [Mueller, 1987; improved by Marion and Bax (1988)]. These coupling constants were used to estimated torsion angles H_α–C_α–C_β–H_β (Bystrov, 1978) for those residues in which a large dispersion of the *J*-values to the two β-protons was observed. A $^3J_{H\alpha,H\beta}$ >9 Hz implies a trans conformation, whereas a small (<4 Hz) $^3J_{H\alpha,H\beta}$ value suggests a $C_\beta H$ in the gauche position relative to $C_\alpha H$ (Pardi et al., 1984; Hyberts et al., 1987). In many cases, $^3J_{H\alpha,H\beta}$ for the gauche $C_\beta H$ was sufficiently small to render the corresponding cross-peak unobservable due to overlap of antiphase multiplet components. Residues having $^3J_{H\alpha,H\beta}$ between 7 and 9 Hz were not constrained since these values could be indicative of the lack of a preferred conformer about the C_α–C_β bond. The information obtained from $^3J_{H\alpha,H\beta}$ (trans, gauche), plus the knowledge of NOEs associated with each $C_\beta H$, permitted the determination of chirality for several C_β protons (Zuiderweg et al., 1985; Hyberts et al., 1987).

Structural Calculation Methods. The distance constraints derived from the experimental NMR data (see above for quantification methods), as well as constraints inherent in the covalent structure of the primary sequence, were used as input for the distance geometry program DSPACE [Hare Research, Inc.; Crippen and Havel (1988) provide a comprehensive re-

Table I: Chemical Shift Values (ppm) for TGF-α (Dex-Val-Val, pH 6.5, 20 °C)[a]

residue[a]	NH	α	β_r	β_s	γ	other
Ser3		3.98	3.81	3.76		
His4	8.41	4.64	3.05	2.98		H4 6.95, H2 8.10
Phe5	8.27	4.96	3.05	2.91		H2,6 7.12, H3,5 7.27
Asn6	8.70	4.92	2.89	2.71		
Asp7*	8.19	4.62	2.48	2.65		
Cys8	8.94	4.25	3.04	3.04		
Pro9*		4.39	1.93	2.15	1.63, 1.63	δ 3.15, 3.03
Asp10	8.58	4.35	2.62	2.62		
Ser11	8.08	4.17	3.77	3.73		
His12	8.34	4.72	3.42	2.75		H2,6 6.58, H3,5 7.93
Thr13	7.71	4.13	4.09		1.20	
Gln14	8.42	4.32	2.05	1.72	2.13, 2.13	
Phe15*	7.87	4.08	3.13	2.85		H2,6 7.11, H3,5 7.17
Cys16	8.31	4.28	1.96	2.45		
Phe17	8.26	4.18	2.65	2.65		H2,6 7.07, H3,5 7.13
His18	6.76	4.42	2.71	2.22		H4 6.84, H2 8.35
Gly19	7.37	3.81 (*s*), 3.47 (*r*)				
Thr20	8.40	4.43	3.87		1.23	
Cys21	9.05	5.15	3.23	3.23		
Arg22	9.42	4.70	1.59	1.50	1.38, 1.38	δ 2.76, 2.71
Phe23*	9.04	4.62	2.62	2.86		H2,6 6.79, H3,5 7.04
Leu24*	8.23	4.41	1.50	1.71	1.49	δ 0.70, 0.68
Val25	8.03	3.62	1.96		1.02, 0.93	
Gln26	8.80	4.04	2.04	2.04	2.35, 2.35	
Glu27*	7.79	4.11	1.66	1.99	2.18, 2.12	
Asp28	7.89	4.20	3.05	2.30		
Lys29	6.89	4.60	1.65	1.50	1.17, 1.17	δ 1.61, 1.58, ε 2.89, 2.89
Pro30*		4.69	1.50	1.65	1.16, 1.16	δ 3.40, 3.23
Ala31	8.84	4.70	1.32			
Cys32*	8.72	5.30	2.56	2.75		
Val33	8.96	4.19	1.95		0.89, 0.81	
Cys34*	9.14	5.00	3.41	2.69		
His35*	8.68	4.83	3.35	2.84		H4 6.98, H2 7.73
Ser36	8.66	4.22	3.87	3.87		
Gly37	8.81	4.11 (*s*), 3.53 (*r*)				
Tyr38*	7.96	5.26	2.89	2.73		H2,6 6.62, H3,5 6.36
Val39	9.19	4.82	2.24		0.81, 0.76	
Gly40	8.11	5.00 (*s*), 3.85 (*r*)				
Ala41	9.25	4.13	1.53			
Arg42	8.71	4.67	2.26	1.29	1.34, 0.70	δ 2.88, 2.88
Cys43	8.05	3.93	2.89	2.39		
Glu44	9.96	4.18	1.57	1.57	1.76, 1.33	
His45*	8.53	5.10	2.97	3.06		H4 7.01, H2 8.12
Ala46	8.74	4.13	1.12			
Asp47	8.08	4.38	2.44	2.17		
Leu48	8.07	4.20	1.53	1.53	1.53	δ 0.841, 0.77
Leu49	8.18	4.27	1.61	1.53	1.54	δ 0.85, 0.77
Ala50	7.59	4.01	1.25			

[a] An asterisk indicates C_β protons that are stereospecifically assigned as *pro-R* (β_r) and *pro-S* (β_s). For those $C_\beta H_2$ protons that are not stereospecifically assigned, the most downfield of the two signals is designated β_r. (*r*) and (*s*) designate non-$C_\beta H_2$ protons stereospecifically defined as *pro-R* and *pro-S*, respectively.

view of the DG algorithm]. Since two regions of β-sheet structure (Gly19–Cys34 and Tyr38–Val39, His45–Ala46) and a type II turn at several pH values (ranging from 3.4 to 9.4) (His35–Tyr38) had been previously established (Brown, S. C., et al., 1989; Tappin et al., 1989; Kohda et al., 1989; Montelione et al., 1989), the hydrogen bonds corresponding to amide protons in slow exchange with H_2O at low pH (Brown, S. C., et al., 1989) were included as constraints. For several residues, information from $^3J_{H\alpha,H\beta}$ and $D_{\alpha\beta}$ NOEs allowed inclusion of H_α–H_β constraints of 2.8–3.0 Å for H_β in the trans configuration and 2.3–2.6 Å for the gauche H_β.

Two stages were involved in calculating a set of final structures. In the first stage, an incomplete set of distance boundaries based on NOEs was used (see above). The stereospecific assignments of CH_2 and CH_3CHCH_3 centers were unknown at this point; therefore, all such centers were defined as nonchiral (Weber et al., 1988). In the program DSPACE, the proton positions were allowed to float between *pro-R* and *pro-S*. A set of five initial structures was calculated. The rough global conformations of these structures enabled the completion of NOE cross-peak assignments (see above), as well as the stereospecific assignments of several C_β centers. The completed distance boundary list was then used in the second stage of calculations.

A combination of the $^3J_{H\alpha,H\beta}$ coupling constants (Table II), the observed NOEs, and the initial structures was used to define the absolute configuration of $C_\beta H_2$ protons of 11 residues as *pro-R* and *pro-S*. The CH_2 protons of five other residues (Gly C_α and Pro C_β) were defined on the basis of observed NOEs and structural restraints alone. $^3J_{H\alpha,H\beta}$ was known for six other residues, but insufficient NOE or structural information was available for definitive stereospecific assignment. For Phe and Tyr aromatic ring protons, free rotation about the CH_2–ϕ bond was indicated by the lack of dispersion of δ and ε resonances. The ring protons were arbitrarily designated δ_1, ϵ_1 on one side of the ring and δ_2, ϵ_2 on the other. Lower bounds were set at 1.8 Å and upper bounds were relaxed to allow the ring to rotate 180°. An upper bound allowing a 360° rotation was not necessary since the ring is symmetrical and the subscript designations are merely for the purpose of

Table II: $^3J_{H\alpha,H\beta}$ (Hz) for $C_\beta H_2$ Protons of TGF-α (Des-Val-Val, pH 6.3, 20 °C)[a]

residue	β_r	β_s	residue	β_r	β_s
Ser3	9	7	Leu24	3	10
His4	7	9	Gln26	*c*	*c*
Phe5	7	9	Glu27	12	4
Asn6	5	10	Asp28	11	4
Asp7	10	5	Lys29	*b*	*b*
Cys8	*c*	*c*	Pro30	*b*	*b*
Pro9	*c*	*c*	Cys32	3	12
Asp10	*c*	*c*	Cys34	5	12
Ser11	*c*	*c*	His35	3	12
His12	*b*	*b*	Ser36	*c*	*c*
Gln14	5	10	Tyr38	12	3
Phe15	5	11	Arg42	*b*	*b*
Cys16	5	11	Cys43	3	12
Phe17	*c*	*c*	Glu44	*c*	*c*
His18	11	5	His45	10	5
Cys21	*c*	*c*	Asp47	11	4
Arg22	*b*		Leu48	*c*	*c*
Phe23	5	11	Leu49	13	5

[a] Only residues possessing a $C_\beta H_2$ center are listed. $^3J_{H\alpha,H\beta}$ values are measured from a PECOSY experiment. Chemical shift values for β_r and β_s are listed in Table I. [b] Unable to measure $^3J_{H\alpha,H\beta}$ due to weak intensity of PECOSY cross-peaks. [c] Unable to measure $^3J_{H\alpha,H\beta}$ due to coincident $C_\beta H$ signals or overlap with another cross-peak.

"bookkeeping". Classification of NOEs to these protons was dependent upon the position of the ring within the initial structure. For example, residues His18, Cys34, His35, His45, and Ala46 exhibit NOEs to the dynamically averaged Tyr38 δ resonance. In the initial structure, residues His18, His45, and Ala46 are situated on opposite sides of the Tyr38 aromatic ring from residues Cys34 and His35, resulting in constraints to δ_1 and δ_2, respectively.

Three strategies were employed to calculate final structures: refinement in DSPACE followed by energy minimization using AMBER 3.0 (Weiner et al., 1984) (DG-MIN); insertion of a molecular dynamics run in AMBER (DG-MD-MIN); and coarse refinement in DSPACE followed by dynamic simulated annealing (Nilges et al., 1988) (DG-XPLOR). All three procedures utilized initial structures generated by the embedding procedure in DSPACE.

In the first strategy (DG-MIN), the DSPACE calculations and refinements were made by using the complete set of constraints (supplementary table S1). The resulting structures were then minimized by the program AMBER 3.0. The second strategy (DG-MD-MIN) involved use of the initial incomplete set of constraints to produce the DSPACE structures (distance geometry calculation and refinements) and subsequent refinement by AMBER molecular dynamics–minization procedures with the complete set of constraints. In the third strategy (DG-XPLOR), using a complete set of constraints throughout, semirefined DSPACE structures (distance violations <1 Å) were refined in XPLOR using both the complete NOE distance set and a set of torsion angles (see Table II) derived from *J*-couplings and local NOEs according to the procedure of Wagner and co-workers (Hyberts et al., 1987).

DG-MIN. A square well harmonic constraint was introduced in AMBER 3.0 for NOE-specified bounds. The minimization was performed in 500 steps with electrostatics turned off to prevent the generation of structural motifs that are overemphasized by charge–charge interactions in the absence of solvent. For this reason, the choice of dielectric is of no concern in these calculations, and the 6-Å cutoff used for the VDW interaction is appropriate. This was followed by 500 steps of minimization with electrostatics turned on. A force constant of 50 kcal/(mol Å) was used for the NOE penalty function. This force constant is strong enough to overcome small energy barriers in the refinement of the structure, but not so strong as to dramatically distort a structure in favor of distance constraints (Brown, F. K., et al., 1989). This was followed by 500 steps of minimization with electrostatics turned on. In all resulting structures, there were no NOE violations exceeding 0.25 Å. The five best (DG-MIN) structures have an RMS deviation in the backbone atoms (defined as H_N, N, C_α, C, O) for residues 16–46 <2.3 Å.

DG-MD-MIN. Eight structures, which were generated in the first stage of calculations (incomplete distance boundary set), showed a variety of orientations of the B loop (Cys16–Cys34) and C loop (Cys34–Ala46) with respect to each other and a RMS deviation of the backbone atoms for residues 16–46 >3.6 Å. These structures were then refined using a MIN-MD-MIN procedure employing the most complete set of NOEs. The MIN-MD-MIN procedure used AMBER 3.0 and was conducted as follows: first, minimization was carried out for 500 steps; the structures were then heated from 0 to 700 K over 3 ps, equilibrated for 5 ps at 700 K, cooled from 700 to 0 K over 3 ps, and concluded with a final 500 cycles of minimization. All runs were done with electrostatics turned off, a nonbonded cutoff of 6 Å, and a force constant of 50 kcal/(mol Å). The RMS deviation of the backbone atoms for residues 16–46 of the best five structures (DG-MD-MIN) is <1.8 Å and residual NOE violations are <0.3 Å.

DG-XPLOR. Fifteen semirefined DSPACE structures were refined with the dynamic simulated annealing procedure (Nilges et al., 1988) using the program XPLOR (Polygen Corp., Waltham, MA). All hydrogens were removed from the DSPACE structures and rebuilt in XPLOR, which ensured proper labeling of all hydrogen atoms and correct configuration of most prochiral carbons in the side chains. In preliminary calculations, the chiralities of most C_β protons were permitted to float. Visual inspection of these structures permitted confirmation of the stereospecific assignments listed in Table I. In the final calculations, the chiralities of these β protons were fixed. In addition to the distance constraints, the torsion angles between the C_α and some C_β protons were fixed in an interval of 30° with a quadratic force field and a force constant of 10 kcal/30°. The force constant for the distance constraints was set to 50 kcal/Å.

Annealing of a typical structure required about 120 min of VAX 8800 CPU time. Rebuilding of the hydrogens in XPLOR ensures proper configuration of all prochiral CH_2 carbons, but this procedure did not fix scrambling of labels on methyl carbons in isopropyl groups in DSPACE structures (Val, Leu), which sometimes caused the dynamic simulated annealing procedure to get trapped in a false local minimum, resulting in incomplete refinement and higher energies. However, swapping of the corresponding methyl labels in the starting structures subsequently led to refinements with low energies and distance violations. The RMS deviation of the backbone atoms for residues 16–46 of the 15 structures (DG-XPLOR) is less than 1.4 Å (80% < 1 Å) with all NOE distance violations of less than 0.4 Å (<0.3 Å in 80% of the structures).

NOESY Back-Calculations. Simulated NOESY spectra were calculated with the program BKCALC (Hare Research, Inc.; Banks et al., 1989) using interproton distances in the final structures. A cross-relaxation rate parameter of -0.07 s^{-1} (provides optimal ratio of cross-peak to diagonal-peak, where resolved), a spin–lattice relaxation time (leakage) of 0.6 s (rough estimate based on overall proton T_1), a cutoff distance of 4.5 Å, and mixing times of 0.15 and 0.30 s were used. The output of BKCALC contains the cross-peaks that are incorporated by the program GNOE into a two-dimensional matrix,

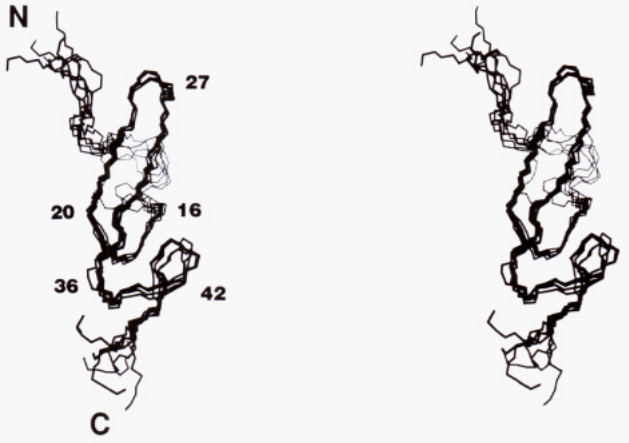

FIGURE 1: Stereoview of six structures obtained with dynamic simulated annealing (XPLOR). The structures were superimposed to minimize the RMSD of backbone atoms of residues 16–46. The three loops are defined as follows: A loop, residues 9–15; B loop, residues 16–34; C loop, residues 34–46.

which is subsequently converted into a FT NMR compatible "smx" matrix. BKCALC was modified to generate, in addition to the spectrum, a combined cross-peak assignment file which depicts the origin of each cross-peak in the back-calculated spectrum.

Results and Discussion

Computational Methods. An NMR template analysis (Hempel, 1989; Hempel & Brown, 1989) was conducted on the most complete set of data. The results of this analysis suggested that residues 1–3, 10–14, and 48–50 should have very little conformational definition while the structure of the remaining residues is more or less well-defined (Hempel & Brown, 1990). This prediction is clearly confirmed by measuring RMS deviations of the 15 DG-XPLOR structures (a superposition of six representative structures is depicted in Figure 1). In these structures, the N- and C-termini vary considerably, and the loop from residues 8 to 15 shows great flexibility. The RMS deviation for backbone atoms (defined as H_N, N, C_α, C, O) of residues 1–15 of the structures shown in Figure 1 is 5.5 Å. On the other hand, the structure of residues 16–47 is highly conserved. The convergence of these structures is not restricted to the backbone atoms; many of the side chains are also well-defined (Figure 2). The RMS deviation for residues 16–46 of the DG-XPLOR structures is >1.4 Å for backbone atoms and >2.2 Å when side chains were included.

To evaluate whether the convergence of these structures is dependent the XPLOR protocol, two other refinement strategies (DG-MIN, DG-MD-MIN) were employed. Structures produced by each of the three strategies are very similar (Figure 3), and when one structure randomly chosen from each approach was overlayed, the RMS deviation of the backbone atoms for residues 16–46 was <1.9 Å.

Structural NOEs. The observed NOE cross-peaks are consistent with the elements of secondary structures reported for TGF-α in previous studies, most of which were conducted

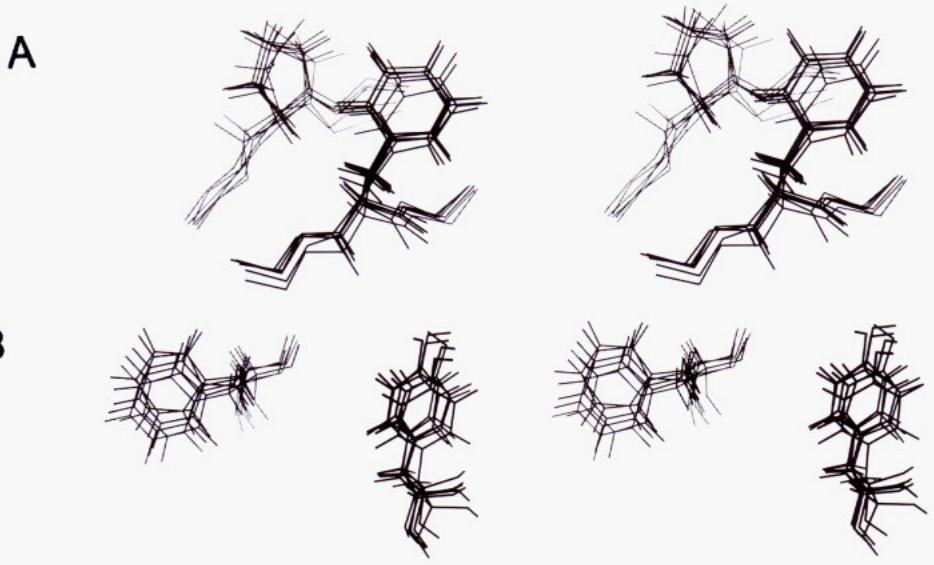

FIGURE 2: Stereoview for the side chains of residues Phe23, Pro30 (A) and Phe17, Tyr38 (B) from DG-XPLOR structures shown in Figure 1.

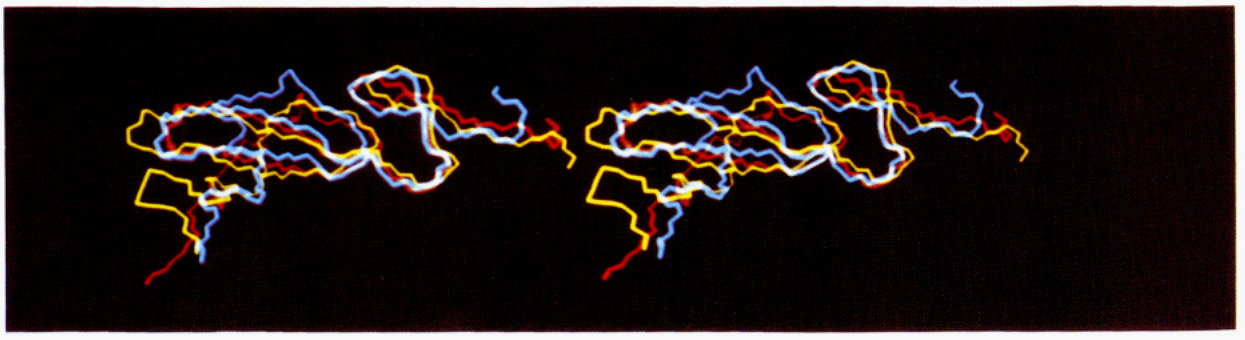

FIGURE 3: Stereoview of the superimposition of one structure from each of the three protocols used: DG-MIN (cyan), DG-XPLOR (red), and DG-MD-MIN (yellow). The structures were superimposed to minimize the RMSD value of backbone atoms for residues 16–46.

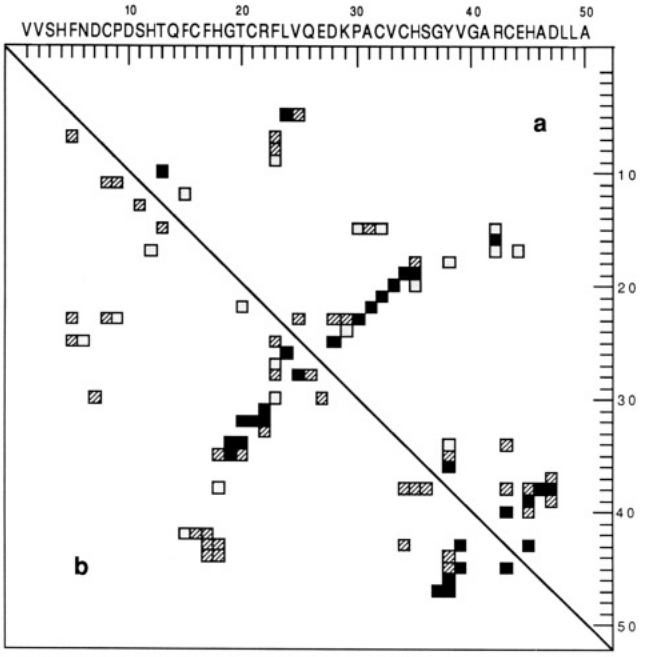

FIGURE 4: Survey of nonsequential NOE-derived distance constraints for TGF-α reported in (a) this paper (pH 6.3, 20 °C) and (b) a previous paper by Kohda et al. (1989) (pH 4.9, 28 °C). Both axes are calibrated with the sequence of TGF-α. Filled, stippled, and hatched squares indicate backbone–backbone, backbone–side-chain, and side-chain–side-chain NOEs, respectively. Where two residues are connected by more than one NOE, the constraint involving the greater number of backbone atoms is shown.

below pH 4 (Tappin et al., 1989; Brown, S. C., et al., 1989; Montelione et al., 1989). However, some differences were reported at pH 6.5 compared to these lower pH values (Tappin et al., 1989) and were confirmed in our laboratory. Many resonances that were broad at pH 3.4 (Brown, S. C., et al., 1989) sharpened at pH 6.3. This occurrence has been attributed (Tappin et al., 1989) to the existence of a tightly folded EGF-like form at near-neutral and high pH and an equilibrium between this structure and at least one other less tightly folded conformer at low pH. The broadening of signals at low pH could be caused by the slow interconversion of conformers at an intermediate rate on the NMR time scale. We also observed NOE correlations at pH 6.3 (not present at pH 3.4) between the N-terminal segment (His4–Asp7) and residues Phe23–Val25, indicating a preference of the relatively flexible N-terminal strand to form a triple-stranded antiparallel β-sheet. However, even at pH $\geq$6.3, the N-terminal residues (Val1–Gln14) remain very flexible, as evidenced by the lack of long-range NOE connectivities in spectra that were collected at a short mixing time (0.15 s) and the averaging of both $^3J_{H\alpha,H\beta}$ couplings to 7 Hz for most of these residues.

The long-range NOEs we observed for TGF-α at pH 6.3 and those reported by Kohda et al. (1989) at pH 4.9 are shown in Figure 4. Although the distribution of NOEs is very similar, indicating little difference in the overall structure, there is some disagreement in the observed individual NOEs. For example, we found correlations between residue Phe15 and residues Pro30–Cys32 and between Phe23 and Pro30 α protons that are not evident in the data of Kohda et al. (1989). These few extra NOEs have a dramatic effect in establishing a well-defined structure which we will demonstrate in a future paper. Also, we observe a $d_{\alpha\alpha}$(5,24) NOE indicative of a short β-sheet between His4–Phe5 and Leu24–Val25. On the other hand, there are correlations presented by Kohda et al. (1989) that are absent in our list of NOE constraints, some of which do not seem to be compatible with our model of the TGF-α structure. For example, we observe no NOEs corresponding to $d_{N\gamma}$(7,30), $d_{N\gamma}$(27,30), or d(23,27) (side chain–side chain). The average distances measured in our model corresponding to these NOEs are 12, 11, and 8 Å, respectively. Most of the remaining extra NOEs in Figure 4b are present at pH 6.3 at a longer mixing time (τ_m = 0.3 s) but were not used as distance constraints in our work.

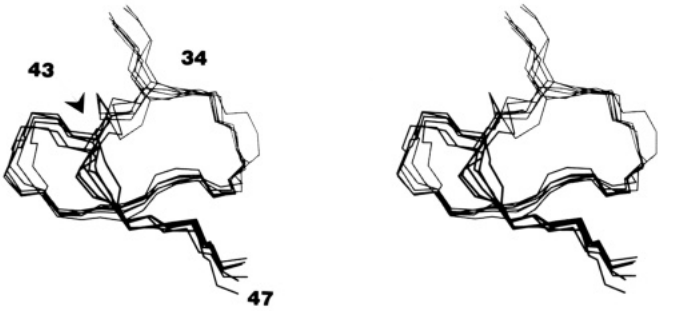

FIGURE 5: Stereoview of the C-loop region Val33–Asp47 depicting an expansion of the structures shown in Figure 1.

At pH 6.3, some of the backbone amide resonances in the region Cys8–Phe15 are weakened by exchange with the solvent, thereby making definite characterization difficult. It should also be noted that there are few NOEs involving any protons (amide, aliphatic, or aromatic) in this region, suggesting that conformational flexibility is probably a more important factor in this region's ill definition than attenuation of amide signals. NOEs, however, are observed between residues Asp10 and Thr13. The loop Phe15–Gly19 is well-defined and has several NOEs to the C-terminal domain (34–46) and to the major antiparallel β-sheet (19–34). Phe15–Phe17 is associated with residues Pro30–Cys32, Arg42, and Glu44. The correlations we have found between this portion of the A loop and the extended β-sheet region (Gly19–Cys34) have not been reported previously. His18 has several connectivities to His35 and Tyr38, while Gly19 is mainly correlated with Cys34 and His35. For the antiparallel β-sheet region from residues Gly19–Leu24 and Lys29–Cys34, most of the expected $d_{\alpha\alpha}$, d_{NN}, and $d_{\alpha N}$ sequential and cross-strand NOE contacts are observed, as well as several cross-strand side-chain interactions. A number of NOEs originate from the side-chain protons of Phe23 and Pro30 to other protons on both sides of the β-sheet, giving this phenyl ring a well-defined conformation in our model as depicted in Figure 2. NOE cross-peaks involving the hairpin loop (Val25–Asp28) are also consistent with those reported previously (Brown, S. C., et al., 1989; Kohda et al., 1989; Tappin et al., 1989), suggesting a type I β-turn (Brown, S. C., et al., 1989).

In the C-terminal domain (Figure 5), NOEs characteristic of an antiparallel β-sheet were exhibited between residues Tyr38–Val39 and His45–Ala46. Asp47 also seems to be part of the well-defined domain as indicated by $d_{\alpha\alpha}$(38,47), $d_{\alpha N}$(38,47), and strong $d_{\alpha N}$(46,47) cross-peaks. Medium-range and sequential NOEs suggest a type II β-turn for the loop (His35–Tyr38) (Brown, S. C., et al., 1989; Tappin et al., 1989; Kohda et al., 1989). There are several connectivities between Cys34–Ser36 and Tyr38. The turn within residues Gly40–Glu44, shown in Figure 4, does not seem to possess a currently named type of bend structure, although it appears to have a well-defined conformation. Of particular interest is a strong d_{NN}(42,43) cross-peak, as well as connectivities from Gly40 H_α to His45 and from Cys43 H_α to Tyr38 and Gly40. Deuterium-exchange measurements at low pH indicated a marginally slow exchange for the amide proton of Gly40, which

might suggest the formation of an intramolecular hydrogen bond. Because there was no clear indication of which carbonyl oxygen might be involved, no hydrogen-bond constraint was defined from the H_N of Gly-40 in our structural calculations. In none of the refined structures did this amide proton appear in the vicinity of a carbonyl oxygen or other potential acceptor. We conclude that there is no identifiable stabilizing hydrogen bond in this nonclassical turn.

Calculated Structures. Comparison of the structures determined in this study with those presented in previous investigations (Kohda et al., 1989; Tappin et al., 1989; Montelione et al., 1989; Katz et al., 1989) reveals many similarities in aspects of secondary structure. Unfortunately, the limited descriptions of the previously published structures prevent us from making detailed comparisons. In order to enable other groups to better evaluate our results, we have made coordinates of our structures available in the supplemental material.

In all but one of these previous studies (Kohda et al., 1989; Tappin et al., 1989; Montelione et al., 1989), the proposed structures were qualitatively deduced from NOE-derived distances. The advantages of a more rigorous, quantitative analysis are evident in several ways. First, the overall tertiary structure, i.e., relationships between β-sheets and turns and between the N-terminal and C-terminal domains, is better defined. Second, one is able to determine the folding of nonclassical structures, particularly turns, where there is no standard pattern of NOEs. Third, the position of the side chains with respect to the backbone and to each other can be known with greater certainty.

Kohda et al. (1989) report correlations between Phe5–Asn6 and Phe23–Val25 but no evidence of β-sheet structure. In their model, the segment Phe5–Phe15 associates with both major β-sheets strands, with residues Asp7 and Pro30 in close proximity. In our calculated structures, six of which are shown in Figure 1, a short stretch of β-sheet is apparent between residues Phe5–Asn6 and part of the major β-sheet Leu24–Val25, forming a triple strand in this region. Other studies suggested the existence of this third strand at pH 6.5 and 9.4 (Tappin et al., 1989) but not at lower pH values (pH <4) (Tappin et al., 1989; Brown, S. C., et al., 1989; Montelione et al., 1989).

The region between residues Cys8 and Gln14 (extending from left to right behind the major β-sheet in Figure 1) is fairly flexible, but in all calculated structures, this segment runs across the two major β-sheet strands at residues Arg22 and Pro30, and residue Asp7 is situated on the opposite side of the β-sheet structure from Pro30. It has been suggested, due to strong d_{NN} NOEs, that a conformation resembling a right-handed helix is adopted for this region, based on analogy with murine EGF (Montelione et al., 1987). Among the calculated structures, a considerable amount of variation exists (see Figure 1). This may be partly due to the weak amide resonances in this region and consequent scarcity of amide NOEs or, more likely, due to conformational heterogeneity. However, in all the structures, a turn involving residues Asp10–Thr13 is indicated. This turn seems to be slightly helical.

The bend involving residues Phe15–Gly19 is not one of the classical types and has not been previously characterized. The calculated structures (Figure 1) indicate a well-defined turn in which the backbone and the side chains show little deviation. The relationships of the Phe side chains to the major β-sheet and to the C-terminal domain are also well determined. The Phe15 ring is positioned between Pro30–Cys32 and Arg42. The structural relationship of the N-terminal domain (Val1–Cys34) with the C-terminal domain (Cys34–Ala50) is manifested predominantly through this region. Residues Phe15–Phe17 correlate with Gly40–Glu44 and Pro30–Val33, while residues His18 and Gly19 are in contact with Tyr38 and Cys34, His35, respectively. The correlations among Phe15–Gly19, Pro30–Val33, and Gly40–Glu44 are necessary to define the relationship between the two "domains" of the protein. Some previous studies also report these interdomain correlations (Kohda et al., 1989; Tappin et al., 1989), whereas others do not (Montelione et al., 1989; Katz et al., 1989). In the latter cases, the global structure of the molecule remains fairly flexible.

An extended antiparallel β-sheet between residues Gly19–Leu24 and Lys29–Cys34 is found in the calculated structures (Figure 1). Models proposed by previous investigations disagree on the impact on the β-sheet structure of the residue Pro30. On the one hand, two studies (Montelione et al., 1989; Tappin et al., 1989) report that Pro30 distorts the β-sheet slightly, leaving the structure intact from Gly19–Leu24 and Lys29–Cys34. In the structure proposed by Kohda et al. (1989), Pro30 completely disrupts the structure and the β-sheet consists only of residues Cys21–Arg22 and Ala31–Cys32. Katz et al. (1989) suggested that Pro30 forms a β-bulge with possible hydrogen-bond formation between Leu24 H_N and Asp28 C=O. Our structure agrees with the first proposition (Montelione et al., 1989; Tappin et al., 1989), i.e., indicating only a small kink in the β-sheet (Figure 1). The extended β-sheet features a distinct right-handed twist of approxmately 90° from end to end. This twist places the loop end of the β-sheet (Val25–Asp28) in a position relative to the remainder of the molecule slightly different from that predicted on the basis of qualitative NOE data interpretation alone. This loop has been previously described as an Ω loop (Katz et al., 1989). Structures generated by all of our calculations (see above) indicate that this loop is a type I β-turn as evidenced by the measured Φ, Ψ angles (Wuthrich, 1986, and references therein).

The C-terminal domain (Figure 5) is composed of two loops (Ser36–Tyr38 and Gly40–Glu44), a short β-sheet (Tyr38–Val39 and His45–Ala46), and a flexible terminus (Ala48–Leu50), consistent with most other proposed models (Tappin et al., 1989; Montelione et al., 1989; Kohda et al., 1989). This structure, however, differs from the antiparallel triple-stranded β-sheet of Katz et al. (1989) from the C loop back to the B loop. We see no evidence for β-sheet formation between Tyr38–Gly40 and Val33–His35. In particular, we found no evidence for the formation of a hydrogen bond involving the H_N of His35 to any acceptor, consistent with the NOE constraints. Moreover, this amide proton is not protected from exchange with solvent water.

The first loop, His35–Tyr38, is a type II β-turn (consistent with observed Φ, Ψ angles) as previously reported (Brown, S. C., et al., 1989; Tappin et al., 1989; Montelione et al., 1989). Structural calculations confirm this assigned secondary structure (Figure 5). The second loop, Gly40–Glu44, although well-defined, cannot be reconciled with a classical type of turn as described above. However, the calculated structures (Figure 5) do indicate that the backbone of this region has a left-handed twist, similar to that observed for mEGF (Montelione et al., 1987). The residue Asp47 extends from the β-sheet (His45–Ala46) and is consistently positioned among the structures. Katz et al. (1989) report a possible hydrogen bond between Asp47 H_n and Glys37 C=O. Our structures demonstrate that these two atoms are consistently in close proximity, thereby supporting this possibility. The Asp47 H_N is not protected from solvent exchange in our studies, probably

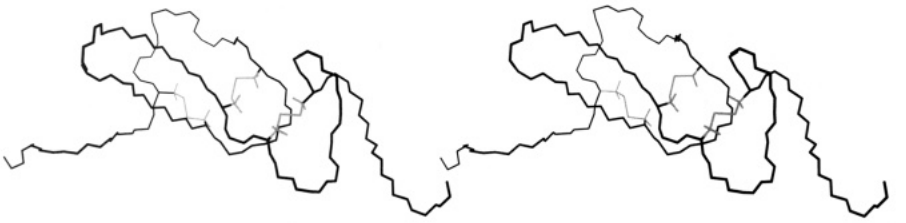

FIGURE 6: Stereoview of the backbone of a single TGF-α structure (DG-XPLOR) demonstrating the relationship of disulfide bridges to the protein structure. Cystines are shown as lighter tracings.

due to "fraying" of the C-terminus if a hydrogen bond is indeed present. The C-terminus Leu48–Ala50 demonstrates considerable flexibility.

The three disulfide bridges are shown as lighter tracings in Figure 6. The disulfide bond between Cys34 and Cys43 depicts a tendency to form a left-handed helical twist (Thornton, 1981). However, the conformations of the linkages between Cys8, Cys21 and Cys16, Cys32 are not well-defined by our NMR data.

Back-Calculations. Few differences were observed between the experimental and simulated NOESY spectra calculated from refined structures. This is illustrated in Figure 7, which shows the experimental and calculated NOEs for the H_α–side-chain proton region. We observed very good qualitative spectral matches from protons that are located in the more rigid region of the protein, i.e., residues Phe15–Ala46. There, for each cross-peak in the NOESY spectrum (Figure 7A), a corresponding peak was found in the back-calculated spectrum (Figure 7B). Furthermore, we found almost no back-calculated cross-peaks that had no experimental counterpart. Most of the extra cross-peaks in Figure 7B originate from the highly flexible regions Val1–Gln14 and Leu48–Ala50 (enclosed in boxes). In each calculated structure, these regions are "frozen" into one conformation which the back-calculation program uses as the basis for distance calculations. Simulated cross-peaks that originate from protons in the structurally conserved region Phe15–Asp47 that are not observed at short mixing times (τ_m ~0.15 s) are enclosed in circles. The corresponding cross-peaks in the experimental spectrum are observed at longer mixing times. A few weak cross-peaks are observed in the experimental spectrum but are not seen in Figure 7A. These NOEs were calculated as very weak cross-peaks and cannot be seen in the plot shown. No attempt was made to adjust the qualitative NOE distance constraints to improve the matches in peak intensities between experimental and back-calculated data. These back-calculated NOESY spectra were valuable during the process of structural refinement, where errors in the constraint lists (mostly typographical) used as input were readily identifiable. Finally, a comparison between back-calculated and experimental spectra provides the best estimate available of the accuracy and precision of the derived structures to the original observable data.

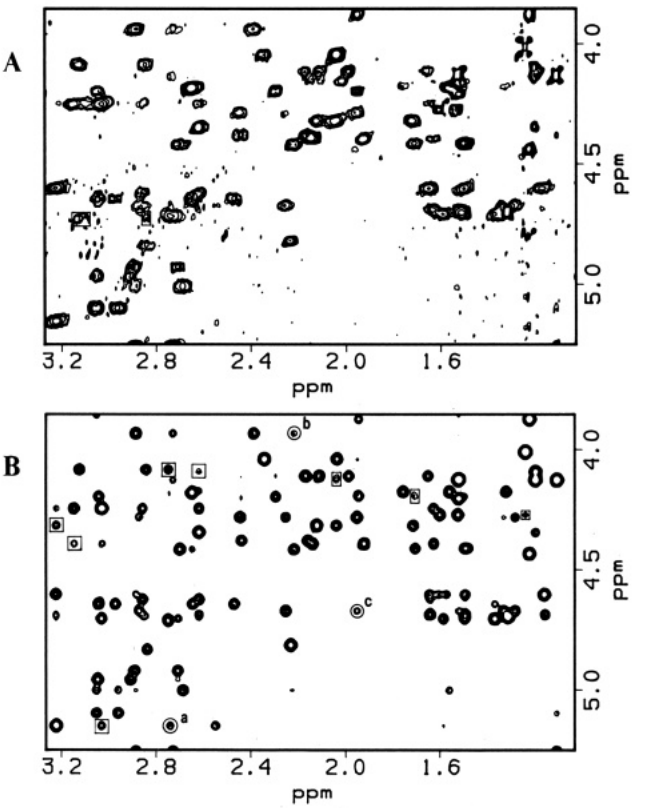

FIGURE 7: Comparison of NOEs between C_α and side-chain protons for (A) a back-calculated NOESY spectrum (τ_m = 0.15 s) based on a DG-XPLOR structure and (B) an experimental NOESY spectrum (τ_m = 0.15 s) of TGF-α. Discrepant cross-peaks orginating from the flexible regions Val1–Gln14 and Leu48–Ala50 are enclosed in boxes. Discrepant cross-peaks originating from the conserved region Phe15–Asp47 are enclosed in circles and correspond to the following proton correlations: (a) Cys21 α–Cys32 β_r, (b) Cys43 α–His18 β_s, and (c) Arg42 α–Cys16 β_r.

Conclusion

TGF-α structures calculated from three different refinement procedures resulted in low NOE constraint violations and small RMS deviations. NOESY spectra calculated from these structures compared well with experimental spectra, indicating that the structures match well with the experimental data and are probably close representations of the structure in solution. Our calculated structures of TGF-α possess many characteristics in common with the structure calculated for mEGF by Montelione et al. (1987), although lack of available coordinates precludes a precise comparison. These include the following: (1) a short triple-stranded sheet involving the N-terminal segment Val1–Asp7 (which, however, appears to maintain some flexibility of the NMR time scale); (2) an irregular, possibly flexible segment Asp10–Phe15; (3) a right-handed twist of the major β-sheet; (4) a type I β-turn at Val25–Asp28; (5) a type II β-turn at His35–Tyr38; (6) a left-handed twist of the loop Gly40–Glu44; and (7) a short antiparallel β-sheet between Tyr38–Val39 and His45–Ala46. A substantial difference is evident, however, in the orientation of the N-terminal and C-terminal domains to each other, due mainly to the lack of observed interdomain NOEs in Montelione et al. (1987). In this respect, the global conformational of our structure more closely resembles that proposed by Kohda et al. (1988) for mEGF. Detailed comparisons of our tertiary structures to others recently proposed for TGF-α (Kohda et al., 1989; Campbell et al., 1989; Katz et al., 1989) must await publication of more details concerning the methods and results of these studies. We have included a complete description of the data in the supplementary material and the structural coordinates have been deposited in the Protein Data

Bank at Brookhaven so that detailed evaluations can be made in the public domain.

ACKNOWLEDGMENTS

We thank Drs. K. Johansen, J. Feild, and M. Anzano for purifying and assaying the protein sample. Mass spectral analysis of the protein was performed by Dr. S. Carr and co-workers. We appreciated the access to the AM600 spectrometer in Dr. Wand's lab at Fox Chase Cancer Research Institute, Philadelphia. L.M. thanks Dr. G. M. Clore for his instructions on XPLOR.

SUPPLEMENTARY MATERIAL AVAILABLE

A table listing distance boundaries input for distance geometry and molecular dynamics minimization and a figure summarizing sequential NOEs found for TGF-α (13 pages). Ordering information is given on any current masthead page.

REFERENCES

Abdullah, N. A., Torres, B. A., Basu, M., & Johnson, H. M. (1989) *J. Immunol. 143*, 113–117.

Banks, K. M., Hare, D., & Reid, B. R. (1989) *Biochemistry 28*, 6996–7010.

Bax, A., & Davis, D. G. (1985) *J. Magn. Reson. 65*, 355–360.

Bothner-By, A. A., & Spevacek, J. (1982) *Pure Appl. Chem. 54*, 569–574.

Brown, F. K., Hempel, J. C., Dixon, J. S., Amato, S., Mueller, L., & Jeffs, P. W. (1989) *J. Am. Chem. Soc. 111*, 7328.

Brown, S. C., Mueller, L., & Jeffs, P. W. (1989) *Biochemistry 28*, 593–599.

Bystrov, V. F. (1978) *Prog. NMR Spectrosc. 10*, 41–81.

Campbell, I. D., Cooke, R. M., Baron, M., Harvey, T. S., & Tappin, M. J. (1989) *Prog. Growth Factors Res. 1*, 13–22.

Crippen, G. M., & Havel, T. F. (1988) *Distance Geometry and Molecular Conformation*, John Wiley & Sons Inc., New York.

Dalvit, C., Rance, M., & Wright, P. E. (1986) *J. Magn. Reson. 69*, 356–361.

Defeo-Jones, D., Tai, J. Y., Wegrzyn, R. J., Vuocolo, G. A., Baker, A. E., Payne, L. S., Garsky, V. M., Oliff, A., & Riemen, M. W. (1988) *Mol. Cell. Biol. 8*, 2999–3007.

DeLarco, J. E., & Todaro, G. J. (1978) *Proc. Natl. Acad. Sci. U.S.A. 75*, 4001–4005.

Derynck, R. (1986) *J. Cell Biochem. 32*, 293–304.

Derynck, R., Goedel, D. V., Ullrich, A., Gutterman, J. U., Williams, R. D., Bringman, T. S., & Berger, W. H. (1987) *Cancer Res. 47*, 707–712.

Hempel, J. C. (1989) *J. Am. Chem. Soc. 111*, 491–495.

Hempel, J. C., & Brown, F. K. (1989) *J. Am. Chem. Soc. 111*, 7323–7327.

Hempel, J. C., & Brown, F. K. (1990) *Biochemistry* (submitted for publication).

Hyberts, S. G., Marki, W., & Wagner, G. (1987) *Eur. J. Biochem. 164*, 625–635.

Kaplan, P. L., & Ozanne, B. (1982) *Virology 123*, 372–380.

Kaplan, P. L., Topp, W. C., & Ozanne, B. (1981) *Virology 108*, 484–490.

Kaltz, B. A., Seto, M., Harkins, R., Jenson, J. C., & Sykes, B. D. (1989) in *Techniques in Protein Chemistry* (Hugli, T. E., Ed.) pp 223–232, Academic, New York.

Kohda, D., Go, N., Hayashi, K., & Inagaki, F. (1988) *J. Biochem. 103*, 741–743.

Kohda, D., Shimada, I., Miyake, T., Fuwa, T., & Inagaki, F. (1989) *Biochemistry 28*, 953–958.

Lazar, E., Watanabe, S., Dalton, S., & Sporn, M. B. (1988) *Mol. Cell. Biol. 8*, 1247–1252.

Lazar, E., Vicenzi, E., Van Obberghen-Schilling, E., Wolff, B., Dalton, S., Watenabe, S., & Sporn, M. B. (1989) *Mol. Cell. Biol. 9*, 860–864.

Marion, D., & Bax, A. (1988) *J. Magn. Reson. 80*, 528–533.

Montelione, G. T., Wuthrich, K., Nice, E. C., Burgess, A. W., & Scheraga, H. A. (1987) *Proc. Natl. Acad. Sci. U.S.A. 84*, 5226–5230.

Montelione, G. T., Winkler, M. E., Burton, L. E., Rinderknecht, E., Sporn, M. B., & Wagner, G. (1989) *Proc. Natl. Acad. Sci. U.S.A. 86*, 1519–1523.

Mueller, L. (1987) *J. Magn. Reson. 72*, 191.

Murthy, U., Anzano, M. A., & Greig, R. G. (1989) *Int. J. Cancer 44*, 110–115.

Nilges, M., Clore, G. M., & Gronenborn, A. M. (1988) *FEBS Lett. 229*, 317–324.

Ozanne, B., Fulton, R. J., & Kaplan, P. L. (1980) *J. Cell Physiol. 105*, 163–180.

Pardi, A., Billeter, M., & Wuthrich, K. (1984) *J. Mol. Biol. 180*, 741–751.

Porchio, A. F., Twardzik, D. R., Bruce, A. G., Wizental, L., Madisen, L., Ranchalis, J. E., Hu, S. L., & Todaro, G. (1987) *Gene 60* (2–3), 175–182.

Rance, M., Sorensen, O. W., Bodenhausen, G., Wagner, G., Ernst, R. R., & Wuthrich, K. (1983) *Biochem. Biophys. Res. Commun. 117*, 479–485.

Tam, J. P. (1987) *UCLA Symp. Mol. Cell. Biol., New Ser. 65*, 7–20.

Tam, J. P. (1988) *Pept.: Chem. Biol., Proc. Am. Pept. Symp. 10th*, 1987, 561–565.

Tappin, M. J., Cooke, R. M., Fitton, J. E., & Campbell, I. D. (1989) *Eur. J. Biochem. 179*, 629–637.

Thornton, J. M. (1981) *J. Mol. Biol. 151*, 261–287.

Todaro, G. J., Fryling, C., & DeLarco, J. E. (1980) *Proc. Natl. Acad. Sci. U.S.A. 77*, 5258–5262.

Twardzik, D. R., Ranchalis, J. E., & Todaro, G. J. (1982) *Cancer Res. 42*, 590–593.

Wagner, G., & Zuiderweg, E. R. P. (1983) *Biochem. Biophys. Res. Commun. 113*, 854–860.

Weber, P. L., Morrison, R., & Hare, D. (1988) *J. Mol. Biol. 204*, 483–487.

Weiner, S. J., Kollman, P. A., Case, D. A., Singh, C. U., Ghio, C., Alagona, G., Profeta, S., & Weiner, P. (1984) *J. Am. Chem. Soc. 106*, 765–784.

Wuthrich, K. (1986) *NMR of Proteins and Nucleic Acids*, Wiley-Interscience, New York.

Zuiderweg, E. R. P., Boelens, R., & Kaptein, R. (1985) *Biopolymers 24*, 601–611.